

Evidence of density waves in single-crystalline nanowires of pyrochlore iridatesAbhishek Juyal,^{*} Amit Agarwal,[†] and Soumik Mukhopadhyay[‡]*Department of Physics, Indian Institute of Technology Kanpur, Kanpur 208016, India*(Received 31 December 2016; revised manuscript received 1 March 2017; published 28 March 2017;
publisher error corrected 31 March 2017)

We present experimental evidence of emergent density-wave instability in single-crystalline low-dimensional wires of yttrium-based pyrochlore iridates. We demonstrate electric-field-induced nonlinear hysteretic switching of the density wave at low temperature, followed by smooth nonlinear conduction at higher temperature ($T > 40$ K) in $Y_{2-x}Bi_xIr_2O_7$, with $x = 0$ and 0.3 . The ac transport measurements reveal the presence of four different collective relaxation processes which dominate at different temperature scales. There is a strong coupling of the normal charge carriers with the density-wave condensate, which is reflected in the linear scaling of the dc conductivity with the collective relaxation rate across a wide range of frequencies and temperatures. The evidence of the density wave in low-dimensional single crystals of pyrochlore iridate could be a precursor to the possible experimental confirmation of the Weyl semimetallic ground state with broken chiral symmetry.

DOI: [10.1103/PhysRevB.95.125436](https://doi.org/10.1103/PhysRevB.95.125436)**I. INTRODUCTION**

The physics of $5d$ heavy transition-metal oxides (TMOs) includes, *inter alia*, a strong spin-orbit interaction (0.1–1 eV) and its interplay with Coulomb correlations. Among the $5d$ TMOs, rare-earth pyrochlore iridates $R_2Ir_2O_7$ ($R =$ yttrium or lanthanide elements) provide a promising experimental test bed to explore the realization of a variety of novel quantum phases [1–3] such as topological Mott insulators [3–5], chiral spin liquids [6], Weyl semimetals (WSMs) [1,7], and axion insulators [1,8] due to the competition between spin-orbit interaction, electron-electron interaction, and the kinetic hopping parameter. Interestingly, chiral symmetry breaking induced by interaction effects in Weyl semimetals can also lead to charge-density waves [9]. However, from an experimental viewpoint, there is very little evidence to either support or disprove such claims.

Earlier experimental studies on pyrochlore iridates have shown the existence of a continuous Mott-insulator-metal transition with increasing lattice spacing induced either by change in the ionic radius of R [10] or by substitutional doping [11], along with evidence of strong correlation without any hard gap at the Fermi level [12]. Similar to the ruthenium pyrochlore systems, this metal-insulator transition in $Y_{2-x}Bi_xIr_2O_7$ is also accompanied by a magnetic phase transition with a small but finite value of spontaneous magnetic moment below the transition temperature [11,13]. The magnetic ground state in some pyrochlore iridates is believed to be spin-glass-like [11,13] as in ruthenium pyrochlores, which develops into a long-range (probably noncollinear) magnetic ordering pattern at low temperatures [1,14] or into a quantum spin liquid as in $Pr_2Ir_2O_7$ [15], although the precise nature of the ordering is not yet fully established [1,16]. The rich variety of quantum phases is most likely to be realized in mesoscopic single-crystalline systems. However, to date, experimental reports on pyrochlore iridates have been mostly confined to bulk single-crystalline or

polycrystalline samples [15,17] and a few reports on epitaxial thin-film growth of iridates [18,19]. For thin films, extraneous factors such as lack of crystallinity, strain, defects, etc., could get in the way of a clear interpretation of the experimental data [19].

In this paper, we present a dc and ac electrical transport study of devices fabricated from *single-crystalline* nanowires of $Y_{2-x}Bi_xIr_2O_7$ (YBIO; with $x = 0.3$) and $Y_2Ir_2O_7$ (YIO). Our study clearly establishes that the electronic ground state of these low-dimensional systems is a charge-density wave (CDW). CDWs are ordered states with broken translational symmetry, with periodic modulations of the electronic charge density accompanied by the associated lattice distortion in systems of electronically reduced dimensions [20]. The density modulation is triggered by an energy-lowering mechanism, a Fermi surface nesting instability (also called Peierls instability) connecting the electronlike part and the corresponding holelike part, thus opening up a gap at the Fermi surface [21,22]. When driven by an external dc electric field, the CDWs are “pinned” below a certain threshold field E_T due to the presence of impurities or an increased surface-to-volume ratio. Below E_T , the transport is Ohmic, with the contribution arising only from “normal” quasiparticles thermally excited above the CDW gap, while above E_T , the CDW slides relative to the host lattice with the collective motion, leading to strong nonlinear transport, with or without hysteretic switching at low temperatures [20].

II. EXPERIMENTAL RESULTS AND DISCUSSION

For this study, we extracted small faceted crystals from the bulk polycrystalline sample surface of YBIO [Fig. 1(a)] by exfoliation. The wire-shaped crystals were transferred on a silicon oxide substrate with prepatterned alignment marks. Atomic force microscopy shows smooth subnanometer crystal surface roughness and a rectangular cross section [Fig. 1(c)]. After locating a suitable crystal, electron-beam lithography was used to form Au/Cr contact pads for electrical measurements [Fig. 1(d)]. For YIO, we observed no such crystal formation on the surface of the pelletized bulk sample. However, sparse quantities of YIO crystals were found in the polycrystalline sample sintered in powder form [Fig. 1(b)]. The

^{*}abijuyal@iitk.ac.in[†]amitag@iitk.ac.in[‡]soumikm@iitk.ac.in

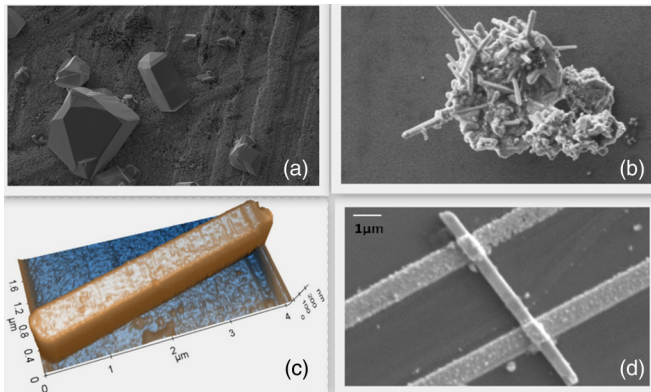


FIG. 1. (a) SEM picture of faceted single crystals of YBIO, loosely attached to the polycrystalline sample surface in contact with air. (b) Cylindrical growth of YIO wires from polycrystalline YIO drop casted on a substrate after annealing at 800 °C. (c) AFM image of a single crystal wire of YBIO isolated from the bulk sample and transferred on a substrate. (d) Representative SEM image of a device with contacts made on the YBIO wire using e-beam lithography.

typical length of these wires varies between 1 and 50 μm , and the diameter is in the range 200 nm to 2 μm . A solution containing suspended YIO crystals was prepared and drop casted on flat silicon oxide substrates, followed by metallization using e-beam lithography. The chemical composition of the crystals of YBIO and YIO was analyzed using energy dispersive x-ray spectroscopy (EDX) and was found to be similar to the respective bulk polycrystalline samples. The details of sample preparation and characterization are given in Ref. [23].

A. The dc response and depinning of density waves

The dc I - V characteristic data of two representative devices based on YBIO and YIO are shown in Fig. 2. Depending on the temperature, the dc I - V characteristics for both YBIO and YIO can be divided into certain distinct regimes. At very low temperature (typically, $T < 40$ K), we find two regimes: (1) Ohmic behavior exists up to certain field value E_T ; (2) beyond E_T , there is a sharp hysteretic switching into a highly conducting nonlinear state. On the other hand, at relatively higher temperature, the hysteresis disappears, leading to three distinct regions in the I - V characteristics: (1) an Ohmic zone below E_T , (2) the appearance of nonlinearity above E_T , and (3) nonhysteretic switching into another highly conducting nonlinear state above E_G ($E_G > E_T$). At still higher temperature, there are two regimes: the Ohmic state followed by a highly nonlinear enhancement of conductance above E_T without any switching. We also find that the current carried by CDW is weakly temperature dependent with a resistive anomaly separating the switching regime and the nonswitching regime near $T \sim 40$ K [see Fig. 2(d)]. The differential conductivity dI/dV curve shown in the inset of Fig. 2(d) simply highlights the switching behavior of the CDW at low T and nonswitching behavior at higher T . However, the CDW persists even beyond the switching regime even for higher T , as seen in the nonlinear conductivity in Figs. 2(a) and 2(b).

From a theoretical perspective, the dynamics of a charge (or spin) density wave is effectively described by the standard

Fisher-Lee-Rice (FLR) model [24], which treats the CDW as a charged elastic object with infinite internal degrees of freedom, deformable around the impurities. The competition between the random impurity potentials trying to pin down the phase of the complex order parameter of the CDW [$\Delta(r,t) = \Delta_0 e^{i\phi(r,t)}$] and the elastic energy of the phase fluctuations leads to interesting dynamics which manifests in the transport behavior. In the *strong-pinning* regime, caused either by a strong impurity potential or by a dilute impurity concentration, the CDW phase is fully adjusted at each impurity site, with the phase-phase correlation length being equal to the average impurity spacing. In the opposite limit of the *weak-pinning* regime arising out of weak impurity potential or large impurity concentration, the CDW phase varies slowly, with its coherence length being larger than the average impurity spacing.

Bistable behavior and hysteresis in the low-temperature dc I - V characteristics of CDWs are a consequence of the elastic deformation of the CDW in the vicinity of pinning centers (impurities) for the critical depinning field E_T . This leads to the backflow of the normal carriers screening the internal electric field [25,26] and is generally modeled by including the coupling between the quasiparticles and the CDW condensate in the FLR model [25–27]. The pinned and electrically driven CDW system first undergoes a transition into a plastically sliding state (at E_{T1}), followed by a second hysteretic transition (at E_{T2}) to a coherently moving CDW state [28]. Alternately, the hysteretic behavior in dc transport of density-wave (DW) based systems can also result from a phase slippage mechanism between weakly coupled CDW domains [29,30].

Although both YBIO and YIO display similar dc characteristics such as hysteretic switching at low temperature and highly nonlinear but smooth dc I - V characteristics at higher temperature, we find a distinct difference between the two so far as the T dependence of E_T is concerned. We find that for devices based on YIO, the threshold field increases sharply with decreasing temperature as T approaches zero (away from the CDW transition temperature), following an exponential dependence $E_T \propto \exp(-T/T_0)$ [see inset of Fig. 2(b)]. On the other hand, E_T for devices based on YBIO is almost independent of temperature [inset of Fig. 2(a)]. The value of E_T is invariably higher in YIO-based devices than in YBIO-based ones of similar dimension. Such temperature dependence of E_T was also observed earlier in standard charge and spin-density-wave systems [31,32] and is associated with thermally induced phase fluctuation and consequent renormalization of the condensate-impurity interaction [33].

Another interesting feature of the dc conductivity is the cooling-rate dependence of the CDW depinning field and the associated nonlinear conduction and switching behavior [see Fig. 2(c)]. This cooling-rate dependence of E_T indicates that the pinning of CDW at low temperature is unlikely to arise from the boundary or surface of the sample or contact effects. The threshold E_T decreases with increasing cooling rate with the eventual disappearance of the switching behavior altogether, leaving only smooth-sliding transition [Fig. 2(c)]. A similar cooling-rate dependence of the CDW state which is otherwise absent in bulk crystals has recently been reported in low-dimensional crystal of $1T$ -TaS₂ [34]. The cooling rate affects the impurity layout as well as the domain growth. Rapid cooling might lead to shrinkage of domains, thus increasing

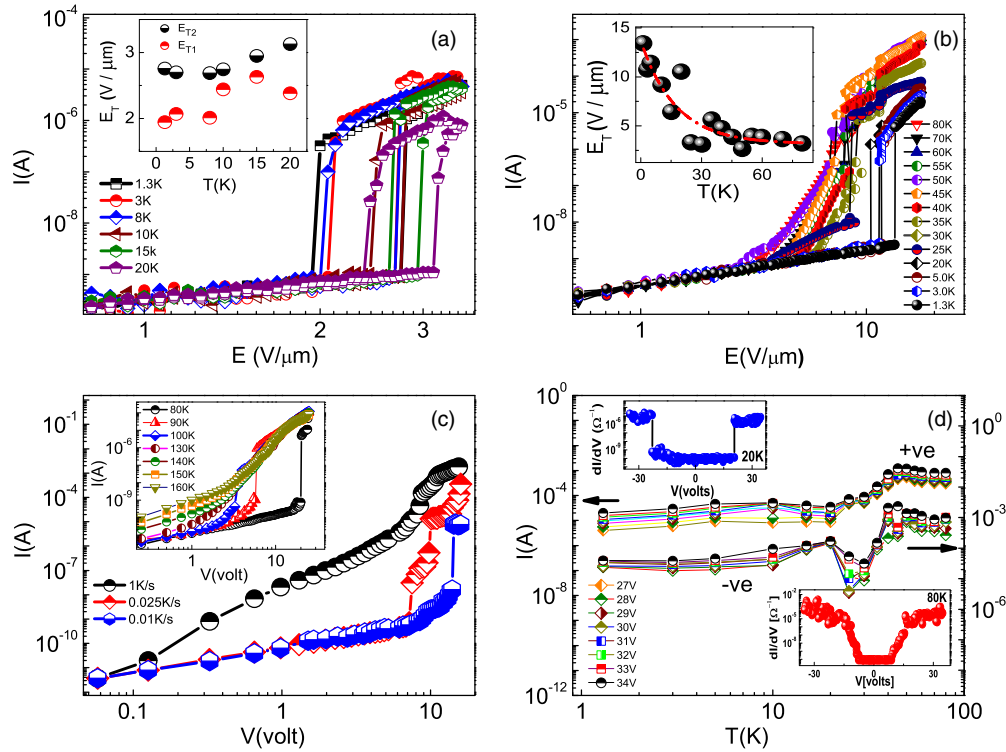


FIG. 2. (a) I - V characteristics of a YBIO single-crystal wire (200×400 nm rectangular cross section) showing hysteretic switching transition at low temperature. The inset shows the depinning threshold field for increasing dc bias (labeled as E_{T1}), which is always greater than that for the decreasing bias (labeled as E_{T2}). (b) I - V characteristics of YIO single-crystal wire (200 -nm diameter) displaying sliding transition of CDW with switching at low T and nonswitching behavior at relatively higher T . Note that the switching behavior at low T ($T \leq 40$ K) is hysteretic (the decreasing field cycle is not shown in for clarity). Inset: The depinning threshold for the increasing dc bias $E_T = E_{T1}$ for low temperatures, far away from the CDW transition temperature, shows an exponential temperature dependence: $E_T \propto \exp[-T/T_0]$, with $T_0 = 17$ K. (c) A representative plot of the cooling rate dependence of depinning threshold for a 2 - μm -diameter YIO wire device. Inset: The dc I - V characteristics at different temperatures. (d) Representative data for the temperature dependence of the current carried by the sliding CDW in YIO at different voltage levels above the depinning threshold for positive and negative biases are shown. The switching and nonswitching regimes are separated by a resistive anomaly (at $T \approx 40$ K).

quasiparticle concentration at the domain boundaries, which in turn could influence the nature of depinning transition. Regarding the temperature dependence of the dc transport, we find that there is no change in the Ohmic resistance below the threshold field with temperature in the low-temperature regime. This suggests that at low temperature, the CDW is primarily pinned by the impurities and the interaction of the CDW with quasiparticles is negligible.

We also studied the dc I - V characteristics of similarly shaped YIO crystals of larger diameter, ~ 2 μm , and found that the Ohmic resistance below the threshold is still temperature independent up to 100 K. However, the threshold electric field for switching decreases with increasing crystal radius (surface-to-volume ratio), similar to that reported for NbSe_3 earlier [35], and the switching is always preceded by a non-Ohmic regime, unlike smaller crystals. If the lateral dimension of the crystal is larger than the transverse phase coherence length of the DW, then the DW can slide around local pinning centers, leading to smooth depinning without switching. The fact that we still observe switching even for a 2 - μm -diameter system suggests that the CDW coherence length is significantly high (≥ 2 μm) in these systems. Note that such large coherence length scales were also reported earlier for other CDW systems such as TaS_3 and NbSe_3 [20,36].

B. Low-frequency dielectric response

Having described the dc transport in CDWs in YIO and YBIO, we now focus on their low-frequency (1 - 10^5 Hz) ac response, up to room temperature. The frequency dependence of the real and imaginary parts of complex conductivity for all the devices at different temperatures was measured using the standard lock-in technique. In Fig. 3(a), we show the real and imaginary parts of the low-frequency dielectric response [related to the ac conductivity via the relation $i\omega\epsilon(\omega) = \sigma(\omega) - \sigma_0$, where σ_0 denotes the dc conductivity] for several temperatures (from 80 to 290 K). The corresponding Cole-Cole plot has a semicircular arc shape [Fig. 3(b)], which suggests a Debye-like dielectric relaxation mechanism. We find that in general the dielectric response at different temperatures follows the generalized Debye relaxation formula [see Fig. 3(c)] of Havriliak and Negami [37,38], which includes a skewed distribution of the dielectric relaxation rates and is given by

$$\frac{\epsilon(\omega) - \epsilon_\infty}{\epsilon_0 - \epsilon_\infty} = \frac{1}{\{1 + [i\omega\tau(T)]^{1-\alpha}\}^\beta}. \quad (1)$$

Here α denotes the temperature-dependent width, β is the skewness of the distribution of dielectric relaxation rates, and $\epsilon_\infty = \epsilon(\omega \rightarrow \infty)$.

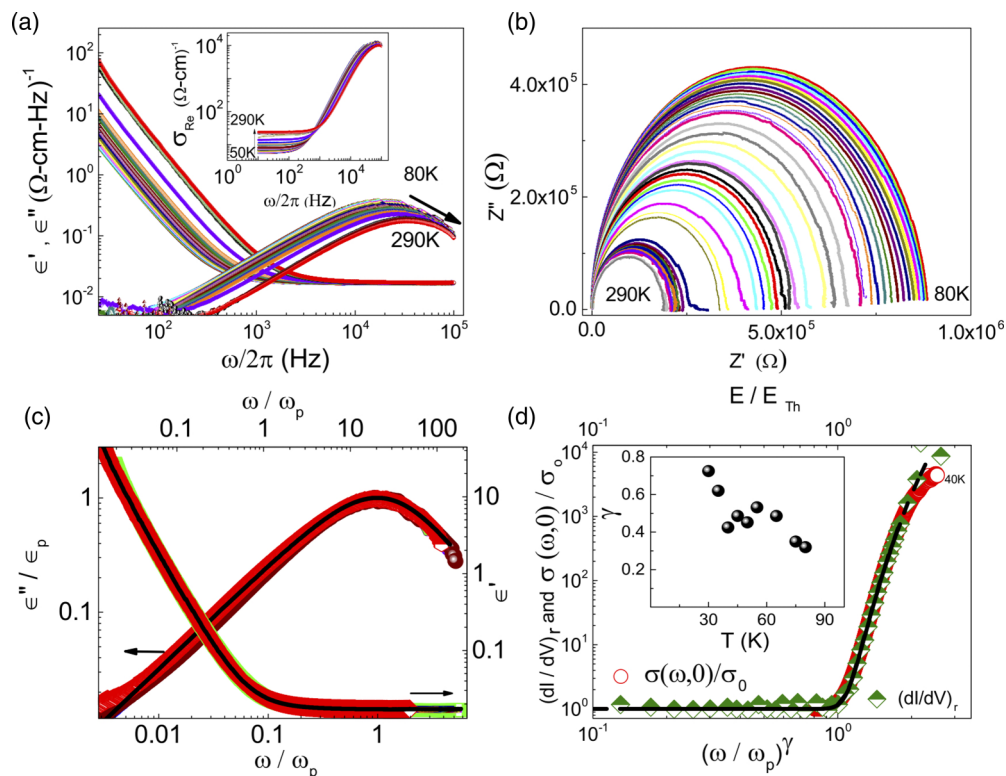


FIG. 3. Dielectric spectroscopy of YBIO for $T > 80$ K: (a) The frequency dependence of the real and imaginary parts of the dielectric constant $\epsilon(\omega) = \epsilon'(\omega) + i\epsilon''(\omega) = [\sigma(\omega) - \sigma_0]/(i\omega)$ at different temperatures from 80 to 290 K. The plot for ϵ'' develops a peak at a T -dependent characteristic frequency $\omega_p = 1/\tau(T)$. The inset shows the real part of the conductivity at different temperatures. (b) The corresponding Cole-Cole plots in terms of the impedance. (c) The scaling of the dielectric response at different temperatures on a universal generalized relaxation curve specified by Eq. (1), represented by the solid black line. Here $\epsilon_p = \epsilon''(\omega_p)$. (d) The frequency dependence of the ac conductivity for YBIO scales with the voltage dependence of the dc conductivity at high temperature ($T \geq 80$ K) with suitable adjustment of the frequency scale defined by the exponent γ . The inset shows the temperature dependence of γ .

Another well-known experimental feature of the pinned CDW transport is the scaling between the dc and the ac conductivities [36,39] at high temperatures for zero dc bias: $\text{Re}\sigma_{\text{ac}}(\omega) = \sigma_{\text{dc}}(V = \gamma\omega)$, where γ is a frequency-voltage scaling parameter, as shown in Fig. 3(d). While one plausible explanation for this scaling is generally given in terms of a photon-assisted quantum-mechanical tunneling model [39,40], this ac/dc conductivity scaling behavior has also been demonstrated numerically for a classical model based on phase pinning [41]. We find the dc/ac scaling relation to be applicable (for $T \geq 80$ K) over a wide range of frequency (with some deviation at high frequency/voltage), with the scaling parameter γ being (almost) inversely proportional to the temperature, as shown in the inset of Fig. 3(d). A similar behavior for the dielectric relaxation at high temperatures (where there is no switching and no hysteresis) in CDWs (and spin-density waves) was also seen earlier in $\text{K}_{0.3}\text{MoO}_3$ [38,42], $(\text{TaSe}_4)_2\text{I}$ [43], polypyrrole nanotubes [44], and $\text{Sr}_{14}\text{Cu}_{24}\text{O}_{41}$ ladder compounds [45].

As T is lowered below 80 K, $\epsilon''(\omega)$ develops an additional peak at higher frequency, marked as Δ_3 in Fig. 4(a). Now this additional peak can also be characterized by Eq. (1), although with a different T dependence of (1) the characteristic scattering time, (2) the relaxation-time distribution parameters α , β , and (3) static dielectric constant ϵ_0 . Further reduction

of T below 40 K leads to the identification of two additional relaxation processes, four in all (labeled Δ_i , with $i = 1, 2, 3, 4$), within the experimental frequency range, 10 – 10^5 Hz [see Fig. 4(a)]. The temperature dependence of τ_i and $(1 - \alpha_i)\beta_i$ for all four different relaxation processes is shown in Figs. 4(b) and 4(c), respectively. The scattering time of all four different relaxation processes follows an Arrhenius temperature dependence ($\tau_i \propto \exp[-T_i/T]$) with a transition temperature of $\{T_1, T_2, T_3, T_4\} = \{2, 8, 314, 348\}$ K. The existence of the two low-temperature scattering/relaxation processes (with $T_2 = 2$ K and $T_4 = 8$ K), which become evident only for $T < 40$ K, is likely to be related to the two bistable phases at low temperature, which results in hysteresis in the dc transport characteristics (see Fig. 2). Similar behavior was observed earlier for CDWs in TaS₃ while exploring the full frequency and T dependence of the dielectric response and was attributed to multiphase glasslike phenomenology, strikingly similar to 3-fluoroaniline [46]. For complete details of the temperature dependence of various parameters of Eq. (1) for each of the four relaxation processes, see Ref. [23].

Figure 4(d) shows the temperature dependence of σ_0 , σ_∞ and the most prominent dielectric relaxation frequency ω_p . Note that $\omega_p = \tau(T)^{-1}$ is also the peak frequency of the $\epsilon''(\omega)$ curve, and it serves as the frequency analog of the threshold field E_T . The prominent relaxation frequency ω_p

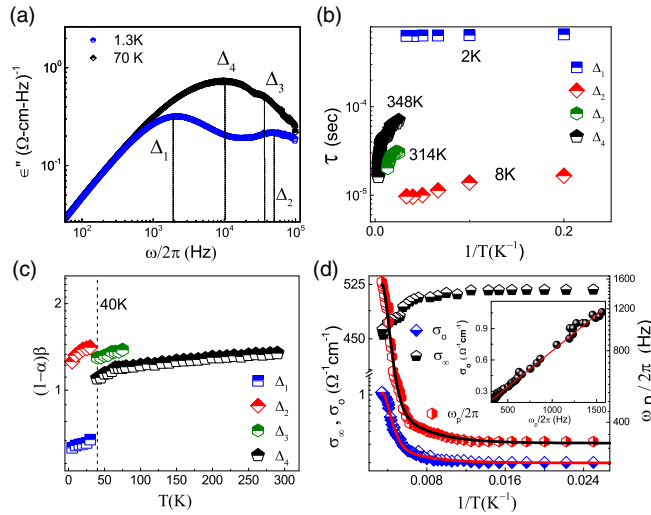


FIG. 4. (a)–(c) Dielectric spectroscopy of YBIO at low T . (a) Appearance of additional relaxation peaks in YBIO in the ϵ'' versus ω plot as the temperature is lowered is shown. (b) Overall, there are four different relaxation rates, characterized by four different τ_i , which follow Arrhenius T dependence with the transition temperatures given by $\{T_1, T_2, T_3, T_4\} = \{2, 8, 314, 348\}$ K. (c) The corresponding temperature dependence of the product of the width $(1 - \alpha_i)$ and the skewness (β_i) of the distribution of the four relaxation rates. (d) The T dependence of the dc (σ_0) and the high-frequency (σ_∞) conductivities, along with the prominent relaxation frequency ω_p as a function of the inverse of temperature in the whole temperature range up to room temperature. The solid black (red) line shows the fit for ω_p (σ_0) obtained by combining the Arrhenius behavior of the four scattering rates τ_i with the corresponding transition temperatures T_i . The dc conductivity follows the activated behavior of the relaxation frequency over a wide range of temperatures and frequencies, as evident from the linear relationship between σ_0 and ω_p shown in the inset.

observed over the entire temperature regime is fitted well by combining the Arrhenius behavior of the four scattering rates τ_i with the corresponding transition temperatures T_i . Further it is evident from the inset of Fig. 4(d) that $\omega_p(T) \propto \sigma_0(T)$. This is a consequence of the longitudinal damped collective charge oscillations in a CDW (polarization built up at the vicinity of the pinning sites) being screened by thermally excited normal quasiparticles [44,45,47]. In fact, we find that $\omega_p/\sigma_0 \approx 0.98 \times 10^4$ Hz Ω cm, and using the relation for the low-frequency longitudinal response which yields $\omega_p/\sigma_0 \approx 4\pi\epsilon_{\text{vacuum}}/(\epsilon_0 - \epsilon_\infty)$ [45], we obtain the relative dielectric constant of YBIO as $\epsilon_0 \approx 1.4 \times 10^{10}$ ($\epsilon_\infty \ll \epsilon_0$), which is consistent with the numbers obtained from the ac data fit using Eq. (1) (see tables in the Supplemental Material [23]). The temperature dependence of σ_∞ calculated from the frequency-dependent conductivity (for YBIO) in the

high-frequency limit [see Fig. 4(b)] is weakly metallic, as expected.

III. SUMMARY

We have presented strong experimental evidence that the ground states of YIO and YBIO are charge-density waves. Unambiguous transport signatures of a conventional density wave have been observed: hysteretic switching at low temperature, orders of magnitude enhancement of dc conductivity in switching and nonswitching I - V characteristics with electric field, scaling of field and frequency-dependent conductivity, strong low-frequency dielectric response, and similar temperature dependence of σ_0 and ω_p . A detailed analysis of the low-frequency ac response revealed the presence of four different relaxation processes, all with an Arrhenius dependence of the relaxation rate, with different transition temperatures. Note that while the experimental data, including the high values of E_T and transition temperature, point towards the existence of a CDW phase, the existence of a spin-density-wave phase at very low temperature cannot be completely ruled out. In addition, due to the presence of strong spin-orbit interaction in pyrochlore iridates, the density wave may actually be a mixture of charge- and spin-density waves. Nevertheless, it seems that the classical FLR model reasonably explains the low- as well as higher-temperature transport behavior, with impurity pinning influencing the CDW dynamics at low temperature and CDW quasiparticle interaction dominating at high temperature.

Regarding the origin of the CDW ground state in low-dimensional pyrochlore iridates, it is not clear whether the underlying mechanism is purely electronic and related to improved Fermi surface nesting or whether orbital effects play any role. Pyrochlore iridates are also expected to host the Weyl semimetallic phase [1,7], and the CDW ordered state is a natural consequence of spontaneously broken chiral symmetry in a three-dimensional WSM and may carry the signature of axion dynamics [9]. Indeed, a magnetic-field-induced charge-density wave at the pinned wave vector connecting Weyl nodes with opposite chiralities in pyrochlore iridates has already been predicted [48]. Since low-dimensional systems lack structural inversion symmetry because of surfaces, chiral symmetry could be broken even without magnetic field. The dynamical axion field may manifest itself as phase fluctuations of the CDW order parameter which couple to the electromagnetic field. Therefore investigating the properties of the density wave and, particularly, its interplay with electromagnetic field would be an effective way of establishing the WSM phase or the axion insulator (AI) phase in pyrochlore iridates. Further experiments are needed to ascertain the nature of coupling of the density wave to the magnetic field. Nonetheless, the experimental observation of the density-wave ground state suggests that realization of a WSM/AI phase in mesoscopic pyrochlore iridates is a distinct possibility.

- [1] X. Wan, A. M. Turner, A. Vishwanath, and S. Y. Savrasov, *Phys. Rev. B* **83**, 205101 (2011).
 [2] B. J. Kim, H. Jin, S. J. Moon, J.-Y. Kim, B.-G. Park, C. S. Leem, J. Yu, T. W. Noh, C. Kim, S.-J. Oh, J.-H. Park, V. Durairaj, G. Cao, and E. Rotenberg, *Phys. Rev. Lett.* **101**, 076402 (2008).

- [3] D. Pesin and L. Balents, *Nat. Phys.* **6**, 376 (2010).
 [4] B. J. Yang and Y. B. Kim, *Phys. Rev. B* **82**, 085111 (2010).
 [5] M. Kargarian, J. Wen, and G. A. Fiete, *Phys. Rev. B* **83**, 165112 (2011).

- [6] Y. Machida, S. Nakatsuji, S. Onoda, T. Tayama, and T. Sakakibara, *Nature (London)* **463**, 210 (2009).
- [7] W. Witzczak-Krempa, G. Chen, Y. B. Kim, and L. Balents, *Annu. Rev. Condens. Matter Phys.* **5**, 57 (2014).
- [8] A. Go, W. Witzczak-Krempa, G. S. Jeon, K. Park, and Y. B. Kim, *Phys. Rev. Lett.* **109**, 066401 (2012).
- [9] Z. Wang and S.-C. Zhang, *Phys. Rev. B* **87**, 161107(R) (2013).
- [10] K. Matsuhira, M. Wakeshima, R. Nakanishi, T. Yamada, A. Nakamura, W. Kawano, S. Takagi, and Yukio Hinatsu, *J. Phys. Soc. Jpn.* **76**, 043706 (2007); D. Yanagishima and Y. Maeno, *ibid.* **70**, 2880 (2001).
- [11] N. Aito, M. Soda, Y. Kobayashi, and M. Sato, *J. Phys. Soc. Jpn.* **72**, 1226 (2003); M. Soda, N. Aito, Y. Kurahashi, Y. Kobayashi, and M. Sato, *Phys. B (Amsterdam, Neth.)* **329**, 1071 (2003).
- [12] R. S. Singh, V. R. R. Medicherla, K. Maiti, and E. V. Sampathkumaran, *Phys. Rev. B* **77**, 201102(R) (2008).
- [13] N. Taira, M. Wakeshima, and Y. Hinatsu, *J. Phys. Condens. Matter* **13**, 5527 (2001); H. Fukazawa and Y. Maeno, *J. Phys. Soc. Jpn.* **71**, 2578 (2002).
- [14] S. M. Disseler, C. Dhital, A. Amato, S. R. Giblin, C. de la Cruz, S. D. Wilson, and M. J. Graf, *Phys. Rev. B* **86**, 014428 (2012).
- [15] S. Nakatsuji, Y. Machida, Y. Maeno, T. Tayama, T. Sakakibara, J. van Duijn, L. Balicas, J. N. Millican, R. T. Macaluso, and Julia Y. Chan, *Phys. Rev. Lett.* **96**, 087204 (2006).
- [16] M. C. Shapiro, S. C. Riggs, M. B. Stone, C. R. de la Cruz, S. Chi, A. A. Podlesnyak, and I. R. Fisher, *Phys. Rev. B* **85**, 214434 (2012).
- [17] V. K. Dwivedi, A. Juyal, and S. Mukhopadhyay, *Mater. Res. Express* **3**, 115020 (2016).
- [18] T. C. Fujita, Y. Kozuka, M. Uchida, A. Tsukazaki, T. Arima, and M. Kawasaki, *Sci. Rep.* **5**, 9711 (2015); T. C. Fujita, M. Uchida, Y. Kozuka, S. Ogawa, A. Tsukazaki, T. Arima, and M. Kawasaki, *Appl. Phys. Lett.* **108**, 022402 (2016); J.-H. Chu *et al.*, [arXiv:1309.4750](https://arxiv.org/abs/1309.4750).
- [19] J. C. Gallagher, B. D. Esser, R. Morrow, S. R. Dunsiger, R. E. A. Williams, P. M. Woodward, D. W. McComb, and F. Y. Yang, *Sci. Rep.* **6**, 22282 (2016).
- [20] G. Grüner, *Rev. Mod. Phys.* **60**, 1129 (1988), and references therein; *Density Waves in Solids* (Addison-Wesley, Reading, MA, 1994); P. Monceau, *Adv. Phys.* **61**, 325 (2012).
- [21] R. E. Peierls, *Quantum Theory of Solids* (Oxford University Press, New York, 1955).
- [22] X. Zhu, Y. Cao, J. Zhang, E. W. Plummer, and J. Guo, *Proc. Natl. Acad. Sci. USA* **112**, 2367 (2015).
- [23] See Supplemental Material at <http://link.aps.org/supplemental/10.1103/PhysRevB.95.125436> for more details about the device fabrication, characterization, and the low frequency dielectric response.
- [24] H. Fukuyama and P. A. Lee, *Phys. Rev. B* **17**, 535 (1978); **17**, 542 (1978); P. A. Lee and T. M. Rice, *ibid.* **19**, 3970 (1979).
- [25] P. B. Littlewood, *Phys. Rev. B* **36**, 3108 (1987); *Solid State Commun.* **65**, 1347 (1988); P. B. Littlewood and C. M. Varma, *Phys. Rev. B* **36**, 480 (1987).
- [26] J. Levy, M. S. Sherwin, F. F. Abraham, and K. Wiesenfeld, *Phys. Rev. Lett.* **68**, 2968 (1992).
- [27] L. Sneddon, *Phys. Rev. B* **29**, 719 (1984); **29**, 725 (1984).
- [28] V. M. Vinokur and T. Nattermann, *Phys. Rev. Lett.* **79**, 3471 (1997); L. Blents and M. P. A. Fisher, *ibid.* **75**, 4270 (1995).
- [29] R. P. Hall, M. F. Hundley, and A. Zettl, *Phys. Rev. Lett.* **56**, 2399 (1986); *Phys. B (Amsterdam, Neth.)* **143**, 152 (1986).
- [30] S. H. Strogatz, C. M. Marcus, R. M. Westervelt, and R. E. Mirollo, *Phys. Rev. Lett.* **61**, 2380 (1988).
- [31] R. M. Fleming, R. J. Cava, L. F. Schneemeyer, E. A. Rietman, and R. G. Dunn, *Phys. Rev. B* **33**, 5450 (1986).
- [32] S. Tomić, J. R. Cooper, D. Jérôme, and K. Bechgaard, *Phys. Rev. Lett.* **62**, 462 (1989); W. Kang, S. Tomi, J. R. Cooper, and D. Jérôme, *Phys. Rev. B* **41**, 4862(R) (1990).
- [33] K. Maki, *Phys. Rev. B* **33**, 2852(R) (1986); K. Maki and A. Virosztek, *ibid.* **39**, 9640 (1989); **42**, 655 (1990); X. Huang and K. Maki, *ibid.* **42**, 6498 (1990).
- [34] M. Yoshida, Y. Zhang, J. Ye, R. Suzuki, Y. Imai, S. Kimura, A. Fujiwara, and Y. Iwasa, *Sci. Rep.* **4**, 7302 (2014).
- [35] J. McCarten, M. Maher, T. L. Adelman, and R. E. Thorne, *Phys. Rev. Lett.* **63**, 2841 (1989); *Phys. Rev. B* **46**, 4456 (1992).
- [36] G. Grüner, A. Zettl, W. G. Clark, and J. Bardeen, *Phys. Rev. B* **24**, 7247 (1981).
- [37] S. Havriliak and S. Negami, *J. Polym. Sci., Part C* **14**, 99 (1966).
- [38] L. Degiorgi, B. Alavi, G. Mihály, and G. Grüner, *Phys. Rev. B* **44**, 7808 (1991).
- [39] J. H. Miller, Jr., R. E. Thorne, W. G. Lyons, J. R. Tucker, and J. Bardeen, *Phys. Rev. B* **31**, 5229 (1985).
- [40] J. Bardeen, *Phys. Rev. Lett.* **42**, 1498 (1979); **45**, 1978 (1980); *Phys. Rev. B* **39**, 3528 (1989).
- [41] L. Sneddon, *Phys. Rev. Lett.* **52**, 65 (1984).
- [42] R. J. Cava, R. M. Fleming, P. Littlewood, E. A. Rietman, L. F. Schneemeyer, and R. G. Dunn, *Phys. Rev. B* **30**, 3228 (1984).
- [43] R. J. Cava, P. Littlewood, R. M. Fleming, R. G. Dunn, and E. A. Rietman, *Phys. Rev. B* **33**, 2439 (1986).
- [44] A. Sarma, M. K. Sanyal, and P. B. Littlewood, *Phys. Rev. B* **91**, 165409 (2015).
- [45] G. Blumberg, P. Littlewood, A. Gozar, B. S. Dennis, N. Motoyama, H. Eisaki, and S. Uchida, *Science* **297**, 584 (2002).
- [46] D. Starešinić, K. Biljaković, W. Brütting, K. Hosseini, P. Monceau, H. Berger, and F. Levy, *Phys. Rev. B* **65**, 165109 (2002).
- [47] J. R. Tucker, W. G. Lyons, J. H. Miller, Jr., R. E. Thorne, and J. W. Lyding, *Phys. Rev. B* **34**, 9038(R) (1986).
- [48] K.-Y. Yang, Y.-M. Lu, and Y. Ran, *Phys. Rev. B* **84**, 075129 (2011).